

## Titanium Nanoparticles Stabilized by Ti–C Covalent Bonds

Debraj Ghosh,<sup>†</sup> Sulolil Pradhan,<sup>†</sup> Wei Chen,<sup>†</sup> and Shaowei Chen\*

Department of Chemistry and Biochemistry, University of California, 1156 High Street, Santa Cruz, California 95064

Received December 3, 2007

Revised Manuscript Received December 19, 2007

Nanosized titanium particles have attracted extensive research interest because of their diverse applications in, for instance, catalysis, energy conversion, and biomedical engineering. Of these, titanium colloids have been used as effective catalysts for the hydrogenation of titanium and zirconium sponges and as a powerful activator for heterogeneous hydrogenation catalysts.<sup>1,2</sup> Titanium nanoparticles have also been used as doping agents to improve the hydrogen storage and exchange properties of sodium alanate, which may find important applications in mobile devices.<sup>3,4</sup> Additionally, titanium nanoparticles formed at the metal–tissue interface may play an important role in the long term stability of titanium-based biomedical implants.<sup>5</sup>

So far various effective protocols have been developed for the preparation of titanium particles. For instance, pulse laser deposition and laser ablation have been used to prepare fine powders of a wide range of transition metals including titanium.<sup>6,7</sup> Yet the core size of the resulting particles is typically of the order of (sub)micrometer. Nanometer-sized titanium particles have been prepared from plasmas in mixtures of titanium tetrachloride, argon, and hydrogen.<sup>8</sup> However, dispersion and chemical processing of the particles remain a challenge. Wet chemistry methods have also been employed to synthesize titanium nanoparticles. For instance, Bonnemann et al.<sup>1,2</sup> used triethylhydroborate as the reducing agent to reduce TiCl<sub>4</sub> into Ti colloids. However, these colloids tended to agglomerate which rendered it difficult to evaluate accurately the size and crystalline structure of the particles. In fact, so far, no clear transmission electron microscopy (TEM) image has been reported of these Ti colloids, to the best of our knowledge.

\* To whom all correspondence should be addressed. E-mail: schen@chemistry.ucsc.edu.

<sup>†</sup> These authors contributed equally to this work.

- (1) Bonnemann, H.; Brijoux, W.; Brinkmann, R.; Dinjus, E.; Fretzen, R.; Jousen, T.; Korall, B. *J. Mol. Catal.* **1992**, *74*, 323.
- (2) Bonnemann, H.; Brijoux, W.; Brinkmann, R.; Fretzen, R.; Jousen, T.; Koppler, R.; Korall, B.; Neiteler, P.; Richter, J. *J. Mol. Catal.* **1994**, *86*, 129.
- (3) Bogdanovic, B.; Felderhoff, M.; Kaskel, S.; Pommerin, A.; Schlichte, K.; Schuth, F. *Adv. Mater.* **2003**, *15*, 1012.
- (4) Fichtner, M.; Fuhr, O.; Kircher, O.; Rothe, J. *Nanotechnology* **2003**, *14*, 778.
- (5) Jonas, L.; Fulda, G.; Radeck, C.; Henkel, K. O.; Holzhter, G.; Mathieu, H. J. *Ultrastruct. Pathol.* **2001**, *25*, 375.
- (6) Dolgaev, S. I.; Simakin, A. V.; Voronov, V. V.; Shafeev, G. A.; Bozon-Verduraz, F. *Appl. Surf. Sci.* **2002**, *186*, 546.
- (7) Barcikowski, S.; Hahn, A.; Kabashin, A. V.; Chichkov, B. N. *Appl. Phys. A: Mater. Sci. Process.* **2007**, *87*, 47.
- (8) Murphy, A. B. *J. Phys. D: Appl. Phys.* **2004**, *37*, 2841.

Thus, in this study, we report the synthesis of stable nanometer-sized titanium particles where the structures of the nanocrystals were unambiguously revealed by high-resolution transmission electron microscopy (HRTEM) measurements. We believe that this is the first of its kind. The particles were passivated by virtue of the strong Ti–C covalent linkages (bond strength 423 kJ/mol<sup>9</sup>). This is largely motivated by recent success of using diazonium compounds as precursors to passivate transition-metal nanoparticles by the strong metal–carbon covalent bonds.<sup>10,11</sup>

We used biphenyl-stabilized titanium nanoparticles as the illustrating example. The biphenyldiazonium compound was synthesized by following a literature synthetic protocol.<sup>12,13</sup> Briefly, a calculated amount of 4-aminobiphenyl was dissolved in ice cold 50% fluoroboric acid. Then a 1:1 stoichiometric amount of sodium nitrite was added into the reaction vessel to generate biphenyldiazonium fluoroborate. The solution was allowed to mix for several minutes. The product was then washed thoroughly with cold fluoroboric acid and ether to remove any impurities.

The titanium nanoparticles were then synthesized.<sup>10,11</sup> In a typical reaction, 0.2 mmol of TiCl<sub>4</sub> was dissolved in 20 mL of tetrahydrofuran (THF). The solution was purged with nitrogen, and the inert atmosphere was maintained for the duration of the synthesis. After 10 min of vigorous stirring, the biphenyldiazonium compound synthesized above was added directly into the reaction vessel. The mixture was allowed to stir for 2 h. Then 5 mmol of superhydride (5 mL of a 1 M solution in THF) was added into the reaction vessel. The solution color changed immediately from brown to dark red, signifying the formation of titanium nanoparticles. The solution was then allowed to stir for 24 h. Excessive free ligands were removed by centrifugation with the addition of ethanol, methanol, and acetonitrile to the synthetic solution. The purified product was denoted as biphenyl-protected titanium (Ti-BP) nanoparticles. Like other monolayer-protected nanoparticles,<sup>10,11</sup> the Ti-BP particles were soluble in apolar organic solvents such as dichloromethane, THF, toluene, and chloroform but insoluble in polar solvents such as methanol and ethanol.

Importantly, while titanium nanopowders have been known for spontaneous combustion upon exposure to air, the obtained Ti-BP nanoparticles were stable under ambient conditions. Thus, no particular protection was needed in the purification process.

The purified particles then underwent thorough characterizations (experimental details in Supporting Information). Figure 1A depicts a representative TEM micrograph of the resulting Ti-BP nanoparticles. The inset shows the corresponding particle size histogram. From the micrograph, it

- (9) Lide, D. R. *CRC handbook of chemistry and physics*; CRC Press: Boca Raton, FL, 2001; electronic edition.
- (10) Mirkhalaf, F.; Paprotny, J.; Schiffrin, D. J. *J. Am. Chem. Soc.* **2006**, *128*, 7400.
- (11) Ghosh, D.; Chen, S. W. *J. Mater. Chem.* **2007**, accepted.
- (12) Yang, H. H.; McCreery, R. L. *Anal. Chem.* **1999**, *71*, 4081.
- (13) Starkey, E. B. *Org. Synth.* **1939**, *19*, 40.

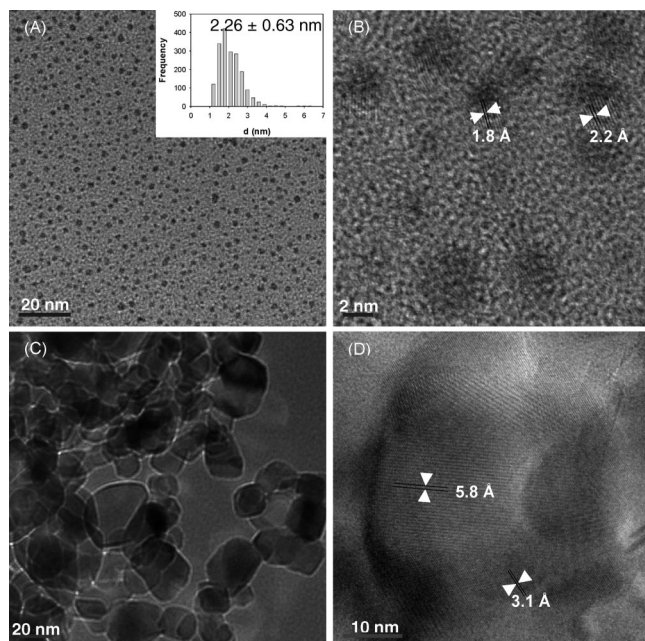


**Figure 1.** (A) Low-resolution and (B) high-resolution TEM micrographs of Ti-BP nanoparticles. Inset to panel A shows the particle core size histogram. (C and D) Corresponding TEM micrographs for TiO<sub>2</sub> particles.

can be clearly seen that the particles are mostly spherical in shape; the fact that the particles were dispersed rather homogeneously on the TEM grid with no apparent aggregation signified good protection of the particle cores by the biphenyl capping ligands through the Ti–C covalent linkages. Additionally, the vast majority of the particles are within the size range of 1–3 nm, with the average core diameter of  $2.26 \text{ nm} \pm 0.63 \text{ nm}$  (consistent results were obtained in atomic force microscopy (AFM) topographic measurements, Figure S3 in Supporting Information). Figure 1B shows the corresponding HRTEM micrograph of the Ti-BP nanoparticles, where well-defined lattice fringes can be seen. The fringes with a lattice spacing of  $2.2 \text{ \AA}$  can be ascribed to Ti(011) and those at  $1.8 \text{ \AA}$  to Ti(012).<sup>14</sup> These observations strongly suggest that the particle cores obtained above are indeed made of metallic titanium. As mentioned above, in previous studies of titanium colloids,<sup>1,2</sup> no clear TEM micrographs have been reported, and thus the morphological details of the colloids have remained largely unknown.

The metallic nature of the Ti-BP nanoparticle cores was further confirmed by comparison to TiO<sub>2</sub> nanoparticles. Figure 1C shows a representative TEM micrograph of TiO<sub>2</sub> nanoparticles, which exhibits an average diameter of about 25 nm. Notably, the lattice spacings for the TiO<sub>2</sub> are significantly different from those of the Ti-BP particles as manifested in panel D by HRTEM measurements. The lattice fringes observed with a spacing of  $3.1 \text{ \AA}$  and  $5.8 \text{ \AA}$  can be attributed to TiO<sub>2</sub>(002) and (200), respectively.<sup>14</sup>

The structures of the Ti-BP nanoparticles were further examined by various spectroscopic techniques. First, similar

(14) JCPDS, International Centre for Diffraction Data; American Ceramic Society Powder diffraction file; The Centre: Newtown Square, PA, 1996.

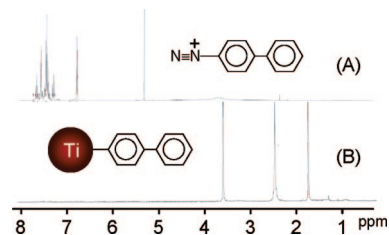


**Figure 2.** <sup>1</sup>H NMR spectra of (A) biphenyldiazonium fluoroborate and (B) Ti-BP nanoparticles. The peak at 3.5 ppm is assigned to methanol and those at 1.8 ppm and 3.8 ppm to THF.

to other transition-metal nanoparticles,<sup>15</sup> the Ti-BP nanoparticles exhibited a featureless UV–vis absorption profile (Figure S1, Supporting Information) due to the Mie scattering effect.

Figure 2 shows the <sup>1</sup>H NMR spectra of (A) biphenyldiazonium tetrafluoroborate and (B) Ti-BP nanoparticles. In panel A, the peaks at 7.3–7.5 ppm are assigned to the hydrogen atoms on the phenyl rings. These peaks disappeared when the ligands were bound onto the particle surface forming Ti–C covalent bonds, as manifested in panel B. Such a phenomenon has been observed previously with other nanoparticle molecules<sup>11</sup> and accounted for by the broadening of the NMR peaks into the baseline. The broadening becomes more pronounced when the functional moieties are situated closer to the particle core. Several structural variables have been used to interpret this, and two significant contributing factors are (i) slow particle tumbling rate in comparison to that of the free ligands and (ii) inhomogeneous packing of the ligands on the particle surface as a result of the nanoscale crystalline facets and curvature of the cores.<sup>16–18</sup> The fact that no sharp features in the range of 7.3–7.5 ppm were observed in the Ti-BP nanoparticles (panel B) also signifies the absence of any excessive free ligands. Thus, the NMR measurements can be exploited as an effective tool to verify particle purity as well (the sharp peaks observed in Figure 2 may be assigned to solvent residuals, e.g., the peaks at 1.8 and 3.7 ppm to THF and that at 5.3 ppm to CH<sub>2</sub>Cl<sub>2</sub>).

In Fourier transform infrared (FTIR) measurements (Figure S2, Supporting Information), the biphenyldiazonium tetrafluoroborate compound exhibited a well-defined vibrational band at  $2250 \text{ cm}^{-1}$ , characteristic of the diazonium moiety, and another one at  $1180 \text{ cm}^{-1}$  of the aromatic C–N stretch. Upon the addition of reducing agents, nitrogen was released, and the remaining biphenyl radicals were bound to the particle cores. Consequently these unique vibrational bands disappeared in the resulting Ti-BP nanoparticles, as demonstrated experimentally (Figure S2), in good agreement with previous studies.<sup>10,11</sup>

Figure 3A shows the current–potential (*I*–*V*) profiles of a Ti-BP nanoparticle solid film deposited onto an IDA electrode surface within the temperature range of 100–300

(15) Creighton, J. A.; Eadon, D. G. *J. Chem. Soc., Faraday Trans.* **1991**, *87*, 3881.

(16) Terrill, R. H.; Postlethwaite, T. A.; Chen, C. H.; Poon, C. D.; Terzis, A.; Chen, A. D.; Hutchison, J. E.; Clark, M. R.; Wignall, G.; Londono, J. D.; Superfine, R.; Falvo, M.; Johnson, C. S.; Samulski, E. T.; Murray, R. W. *J. Am. Chem. Soc.* **1995**, *117*, 12537.

(17) Badia, A.; Singh, S.; Demers, L.; Cuccia, L.; Brown, G. R.; Lennox, R. B. *Chem. Eur. J.* **1996**, *2*, 359.

(18) Song, Y.; Harper, A. S.; Murray, R. W. *Langmuir* **2005**, *21*, 5492.

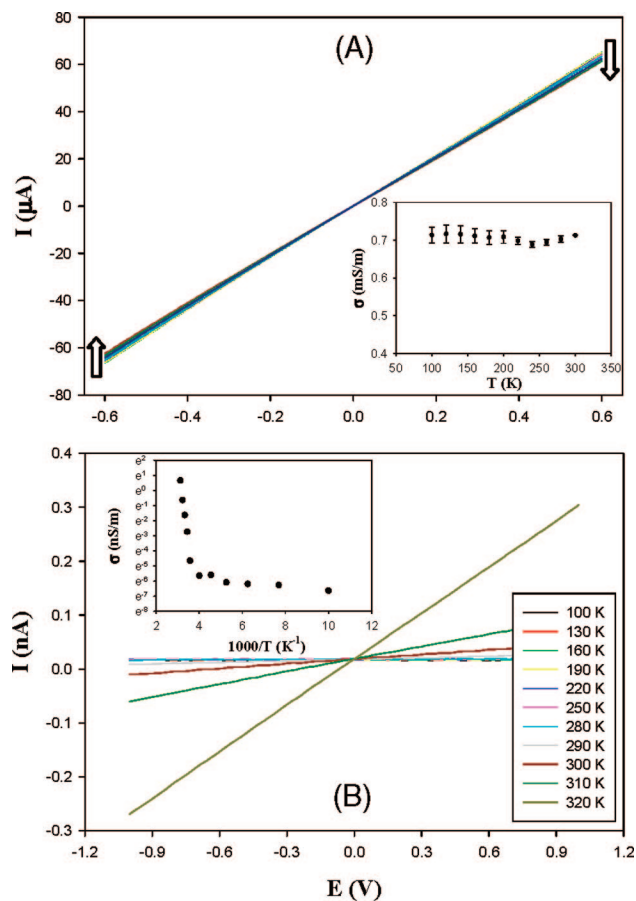


**Figure 3.** Solid-state current–potential profiles of a dropcast film of (A) Ti-BP nanoparticles and (B) TiO<sub>2</sub> particles within the temperature range of 100–300 K. Potential scan rate 20 mV/s. Insets depict the respective variation of the film conductivity with temperature.

K. It can be seen that the  $I$ – $V$  curves are highly linear (ohmic) in the potential range of  $\pm 0.6$  V, most likely because of the short and aromatic biphenyl moieties that serve as the barrier for interparticle charge transfer. The electronic conductivity evaluated from the slopes of the  $I$ – $V$  curves is of the order of  $10^{-3}$  S/m, which is about 9 orders of magnitude smaller than that of pure metallic titanium ( $2.56 \times 10^6$  S/m at 273 K).<sup>9</sup> More interestingly, the figure inset appears to show a small decrease of the conductivity with increasing temperature, a behavior typically anticipated for metallic materials. We observed similar behaviors with Pd-BP nanoparticles (in fact, their conductivity is very comparable), but not with particles passivated by thiol derivatives, which was partly accounted for by the strong metal–carbon covalent linkages and low contact resistance.<sup>11</sup>

By contrast, the conductivity properties of the TiO<sub>2</sub> nanoparticles are significantly different. Figure 3B depicts the  $I$ – $V$  curves of a TiO<sub>2</sub> nanoparticle solid film prepared in a similar fashion under identical experimental conditions. Because of the semiconducting nature of the TiO<sub>2</sub> particles (bandgap  $\sim 3$  eV),<sup>19</sup> the currents measured within the

potential range of  $\pm 1$  V are about 3 to 4 orders of magnitude lower than those of the Ti-BP nanoparticles (panel A), despite the substantially larger core size, the absence of an organic capping shell, and the higher potential bias (note the different current scales in Figure 3). As the applied potential bias is smaller than the particle bandgap, the currents are most likely arising from particle surface defects (trap states) that facilitate interparticle charge transfer.<sup>20</sup> Overall, the particle conductivity increased with increasing temperature, as manifested in the inset to panel B, suggesting that the interparticle charge transfer follow a thermal activation mechanism. Similar behaviors have been observed extensively in previous studies with other nanoparticles that are stabilized by thiol derivatives.<sup>16,21–23</sup>

Comparison of the particle ensemble conductivity under photoirradiation further distinguishes the metallic Ti-BP particles from the semiconducting TiO<sub>2</sub> particles. Experimentally, lasers of different wavelengths (from 638 to 355 nm) were shone onto the particle films, and the corresponding  $I$ – $V$  characteristics were measured. For the TiO<sub>2</sub> particle films, drastic enhancement of the conductance was observed upon photoexcitation, which was interpreted by an increase in the concentration of charge carriers,<sup>20,24</sup> whereas the  $I$ – $V$  responses of the Ti-BP particles remained virtually invariant with laser photoillumination (Figure S4, Supporting Information).

In summary, we report the synthesis and characterization of metallic titanium nanocrystals that were stabilized by Ti–C covalent linkages. With semiconducting TiO<sub>2</sub> nanoparticles as the control, the metallic nature of the Ti-BP particle cores was visibly confirmed by HRTEM measurements. Additional characterizations by various spectroscopic techniques further supported the notion that the particles were passivated by metal–ligand covalent bonds. The particles exhibited interesting solid-state conductivity properties that were consistent with metallic materials, in sharp contrast to the semiconducting TiO<sub>2</sub> nanoparticles.

**Acknowledgment.** We thank the National Center for Electron Microscopy at the Lawrence Berkeley National Laboratory for use of its facilities. This work was supported in part by the National Science Foundation (CHE-0456130 and CHE-0718170).

**Supporting Information Available:** UV–vis and FTIR spectra, AFM topographic images, and photoconductivity profiles of the Ti-BP and TiO<sub>2</sub> nanoparticles (PDF). This material is available free of charge via the Internet at <http://pubs.acs.org>.

CM703423K

(20) Pradhan, S.; Chen, S. W.; Wang, S. Z.; Zou, J.; Kauszlarich, S. M.; Louie, A. Y. *Langmuir* **2006**, *22*, 787.

(21) Wuelfing, W. P.; Murray, R. W. *J. Phys. Chem. B* **2002**, *106*, 3139.

(22) Doty, R. C.; Yu, H. B.; Shih, C. K.; Korgel, B. A. *J. Phys. Chem. B* **2001**, *105*, 8291.

(23) Snow, A. W.; Wohltjen, H. *Chem. Mater.* **1998**, *10*, 947.

(24) Sugimura, H.; Uchida, T.; Shimo, N.; Kitamura, N.; Masuhara, H. *Mol. Cryst. Liq. Cryst. Sci. Technol., Sect. A* **1994**, *252*, 497.

(19) Nozik, A. J.; Memming, R. *J. Phys. Chem.* **1996**, *100*, 13061.